IEEE Access
Multidisciplinary | Rapid Review | Open Access Journal

Received 29 October 2025, accepted 24 December 2025, date of publication 5 January 2026, date of current version 16 January 2026.

Digital Object Identifier 10.1109/ACCESS.2026.3651163

RESEARCH ARTICLE

Coherent Electro-Thermal Qualification of the Insulation System for Electrical Machines

A. RUMI[1], L. ZANOTTI[2], A. CAVALLINI[3], (Fellow, IEEE), AND P. SERI[3], (Member, IEEE)
[1]Coveme S.p.A., 40068 San Lazzaro di Savena, Italy
[2]Private Consultant, 40136 Bologna, Italy
[3]Department of Electrical, Electronics, and Information Engineering, University of Bologna, 40136 Bologna, Italy

Corresponding author: P. Seri (paolo.seri2@unibo.it)

ABSTRACT Qualification of inverter-fed electrical machines through the procedure suggested in the IEC std. 60034-18-41 entails the application of thermal, mechanical, and ambient stresses, followed by measuring partial discharges (PD-proof test). For practical reasons, stress factors are applied sequentially, and measurements are conducted on the machine at room temperature. This procedure is simple but has two major limitations. The first is that testing will not activate synergies between stresses. The other one is that partial discharge inception voltage measurements under impulsive voltages sometimes provide overly optimistic results. This paper suggests an alternative procedure to conduct the qualification of inverter-fed machine insulation. The proposed procedure combines electrical and thermal stress, thus accounting for their synergies. As the applied electrical stress is like that experienced in service, partial discharges can be initiated during aging. This might lead to failure without the need for testing partial discharge.

INDEX TERMS Inverter-fed electrical machines, partial discharges, qualification.

I. INTRODUCTION

Electrification is pushing electric motor design, materials, and control systems to attain more efficient, reliable, and compact electric motors [1], [2], [3]. These improvements have expanded the range of applications where electric motors can be used effectively, such as in water transportation, aircraft [4], [5] and space vehicles -where reliability and power density are key factors. As technology continues to advance and creative minds explore new possibilities [6], [7], electric motors find novel applications that redefine the requirements that manufacturers must satisfy to stay in the market. Usually, applied stresses (i.e., electrical, thermal, and mechanical) are pushed to higher levels. This calls for the adoption of novel solutions, with careful attention to the desired life target of that specific product, which becomes increasingly tightly bound to a specific application, rather than a whole kind.

With the adoption of tailored solutions, one problem arises about machine insulation qualification. IEC 60034-18-41 [8] suggests to qualify the insulation system through accelerated testing, with stress levels that might not be representative of a novel application. The associate risk is the over- or under-representation of one or more stresses, thus initiating or not the same degradation processes active in operation. A coherent testing procedure should thus be devised.

"Coherent testing" refers to a systematic approach to accelerated aging that minimizes deviations from representative operating conditions by ensuring a thermodynamically consistent and electrically accurate stress environment. The word "coherent" here means that the selected stress levels are large enough to accelerate aging, but not so large to introduce degradation processes that are not active in operation. Dealing with electro-thermal stress, the electrical stress should be comparable to or larger than that in operation. Similarly, temperatures should be sufficiently high to expedite thermal aging without triggering unreasonable chemical reactions. Regarding electrical stress, the pass criterion in [8] requires partial discharge inception voltage (PDIV) to be above the test voltage. Indeed, PDIV is remarkably affected by the characteristics of the applied voltage waveform and temperature, sometimes in non-trivial ways [9], [10], [11], [12], [13]. Accordingly, a coherent test setup must also reproduce

The associate editor coordinating the review of this manuscript and approving it for publication was Ruisheng Diao.

as closely as possible the distribution of both electrical and thermal stress in operation.

If the concept of a realistic testing scenario is pushed forward, the experimental setup should be able to expose the insulation models (or complete stators) to both electrical and thermal stresses simultaneously. In [8], sequential testing is suggested for practical reasons. Sequential stress application, as outlined in IEC 60034-18-21 [14], remains a practical and well-established method for evaluating the temperature capabilities of industrial machines and offers a more cost-effective alternative when resources are constrained. However, simultaneous testing should be preferable when possible (e.g. if testing cost is not a factor), as it allows for the detection of potential synergistic aging mechanisms from simultaneous applications of all stress factors (multifactor test) [15], [16], [17], [18], [19].

In summary, the sequential qualification procedures supported in [8] and [14] are becoming more and more unsuitable for modern applications and for the current market fragmentation. However, extensive testing of full-size motors, with full size power, perfectly replicating the final application would be an unreasonable requirement. This paper proposes a simple yet effective technique to produce coherent electro-thermal stress distributions on stators as a tool to improve electrical insulation system qualification. This greatly reduces the investment needed during qualification in terms of time, equipment and eventually money while being able to provide more realistic results as synergies between thermal and electrical stresses are accounted for.

The next sections will discuss: the state of the art for different scenarios (Section II), a theoretical discussion of the proposed method developed to overcome the current limits (Section III), and its experimental validation through a case study (Section IV).

II. ENSURING MACHINE RELIABILITY

A. POSSIBLE ROUTES FOR ASSESSING MACHINE RELIABILITY

Reliability tests should be conducted in test benches consisting of motor/load cell pairs to attain a multifactor stress profile, as experienced in operation. This approach has practical drawbacks. On the one hand, the system would be expensive (the bench should feature an energy recovery system to avoid considerable energy consumption, and it must be soundproof and safe). On the other hand, it would take an exceedingly long time to assess reliability as thermal aging would not be accelerated since mechanical parts like bearings and their lubricants cannot operate at the temperatures required for the insulation accelerated thermal test (e.g., 150°C).

Another approach involves conducting qualification tests on insulation models as outlined in [8], which involves aging cycles followed by diagnostic cycles. During the aging cycles, thermal, mechanical, and ambient stress are imposed on the insulation system, as in [8]. The diagnostic cycles involve PD-proof tests, which can be affected by potential inaccuracies. On one side, these tests may be affected by variance, such as a lack of starting electrons. On the other side, the effects of operating temperatures are simulated by increasing the test voltage using a safety factor (indicated in [8] as an enhancement factor). However, this factor may not accurately capture the variations in dielectric permittivity and clearances of the insulation system at operating temperatures.

Another factor that differentiates qualification tests from aging in operation is that aging factors are applied sequentially, where as a multifactor aging should be preferred as specified in [15]. Mechanical and ambient aging cycles require specialized equipment and are hard or expensive to include in a multifactor aging test. On the contrary, thermo-electrical aging test can be realized with an acceptable effort. However, to get results in a reasonable amount of time, the aging temperature must be raised above the class temperature [14]. This might reduce the PDIV below the levels reached in operation, where the class temperature is hardly reached. If the intended life of the insulation system is low (see e.g., motorsport specifications), a test at a temperature comparable to the operating temperature can be conducted. However, in most cases, that will not be possible. In those cases, a two-stage aging procedure can be envisaged (Fig. 1):

1. Thermal aging at a temperature decided based on [14]
2. Electro-thermal aging at the operating temperature. During this stage, aging will be mostly electrical, while thermal aging will be negligible.

While this investigation concentrates on electro-thermal aging to facilitate an accelerated qualification process accounting for stress synergies, it is acknowledged that mechanical vibration and humidity significantly influence the long-term degradation mechanisms in real-world applications. Accordingly, the approach proposed here can be part of a more complex accelerated aging procedure involving electrical, thermal, mechanical, and ambient stresses. The evidence reported in the following supports a detailed examination of the synergies between electrical and thermal stresses and offers a viable path toward a practical accelerated test. Future work will explore methods to incorporate, or simulate, the effects of mechanical vibration and humidity to further enhance the fidelity of the qualification methodology.

In the following, focus will be on stage 2, as it requires particular care to ensure that the electrical stress is comparable to that experienced in operation.

This method can provide a more focused and accelerated assessment of insulation degradation compared to the comprehensive, albeit time-consuming, IEC standard. By concentrating on critical voltage stress, it enables quicker identification of failure mechanisms while acknowledging the absence of partial discharges. Indeed, it can become an integral part of the procedure suggested in 60034-18-41.

B. PROPOSED METHOD

Reference is made here to stator mockups replicating the stator of the machine (often replacing iron with aluminum and avoiding introducing the rotor).

To simplify the experimental setup and facilitate focused investigation of electro-thermal stress, the stator mockup was tested without incorporating a rotor. While the presence of a rotor would introduce counter-electromotive forces influencing stator coil voltage waveforms, accurately replicating these effects universally is impractical. In the proposed setup, voltage stresses are not mitigated by the rotor counter-electromotive force. Thus, using pulsed voltage waveforms provides a worst-case scenario.

For combined thermo-electrical aging stress cycles, two main routes can be considered:

1. With voltage stress levels equal to the service ones.
2. With voltage levels higher than the service ones, but lower than the PDIV of the pristine stator, to avoid too early inception of partial discharges that would provide unrealistic results.

The first approach will be explored in the following, as it enables using commercial inverters with DC bus voltage and switching frequency like those used in service.

This approach poses a main issue. Stator mockups are not equipped with rotors. In the absence of the counter-electromotive forces generated by the rotor rotation and without significant changes to the inverter control, the currents flowing through the windings are limited only by their impedance (Z_{ph}, which is too small to cause an important voltage drop). Thus, the joule losses in the winding would be both unrealistic and unacceptable.

The solution to this issue is to limit the stator currents using resistors whose potential drop can be compared to that caused by the presence of the counter-electromotive force. They can be inserted in series to the windings, before the star point (if accessible, which is normally the case when using statorettes). This approach requires lower power to operate, enabling the use of inexpensive voltage sources.

In this work, the test setup consisted of the stator mockup mounted within an oven to enable independent control of the winding temperature. A resistance, with value chosen (see section IVa) to limit the current to $1A_{RMS}$, was connected in series with each phase of the stator windings. This strategy and its consequences on the electrical stress experienced by each insulation system in a rotating machine will be explored in the next chapter.

III. THEORETICAL IMPLICATIONS

The addition of series resistors with impedance Z_0 to phase windings will alter the voltage profile experienced by insulation systems. Consider the schematic representation of Fig. 2, which represents a common operating condition, with one phase connected to the positive pole of the DC bus, while the others are connected to the negative pole. The following will also hold for all possible configurations associated with common commutation schemes.

Theoretically, if $Z_0 = Z_{ph}$ the voltage drop on resistors should match that of each phase winding. This would imply that the electrical stress imposed on each insulation system of the machine would be about halved. Though windings will have a much more inductive characteristic than shunting resistors, and each branch for each phase will behave similarly to a series RL circuit. Hence, during commutations, the coil impedance will dominate, and the phase-to-neutral voltage drop will be found mostly on windings. After a certain time from commutation, the phase-to-neutral voltage will reach a plateau, and the voltage drop will shift onto the shunting resistors.

During commutations, the peak-to-peak and rise time of the voltage across each coil will be like that experienced in operation (Fig. 3). Thus, the likelihood of PD inception will be the same for testing and operation. This was established by previous works [20], [21] and does not constitute a limitation of the proposed methodology, which holds its validity for testing of phase-to-phase, phase-to-ground, and turn-to-turn insulation systems.

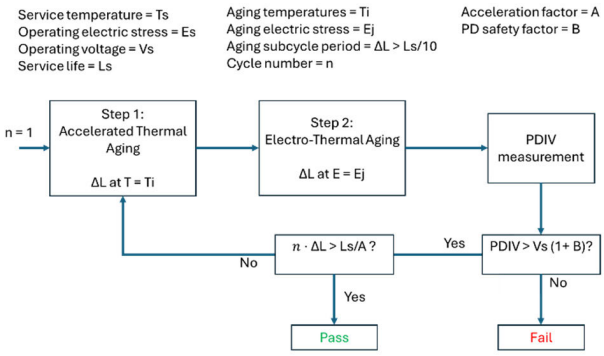

FIGURE 1. Schematic representation of a series of complex sequential subcycles aimed at the accelerated qualification of an electrical insulation system subject to thermal and electrical stresses, after [8], [14], [15].

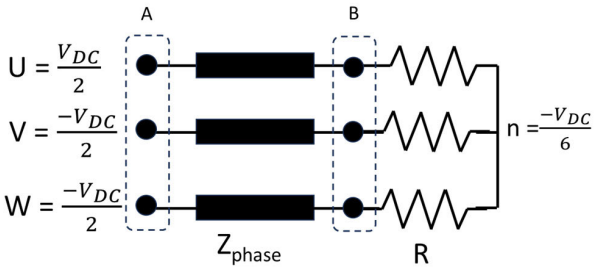

FIGURE 2. Connection scheme and potential at the terminals and star point of the insulation system model. Z_0 represents characteristic impedance.

An important aspect to consider is the peak voltage found at the interconnections between a coil and a resistor (points "B" in Fig. 2). The voltage at those interconnections will be influenced not only by the switching of the respective phase but also by the voltage at the star point (which fluctuates

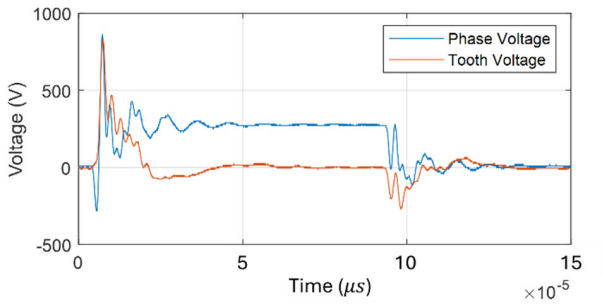

FIGURE 3. Phase and coil voltages with 500 Ω series resistance. The measured voltages represent the response of the system to an applied square voltage excitation of an individual coil within the stator. Voltage oscillations likely correspond to resonances associated with the winding's inductance and capacitance.

following the switching of the other phases), potentially overstressing part of the phase to ground insulation with a transient voltage. At those points, a peak voltage of, for example, $V_{DC}/2$, should be expected during normal operation, while in the presence of series resistors, the same insulation would experience $2/3V_{DC}$.

Overshoot and ringing shall be expected at the ''inverter side'' of the setup (points ''A''), especially in the presence of high slew rates or long connecting cables. Since these overshoots are characterized by high frequency components, they will affect the turn-to-turn voltage stress at the line side of a coil, while their effects will be reduced downstream (points ''B'') due to windings acting as RL low pass filters [13]. If voltage overshoots are considered, point A will experience a peak stress equal to $V_{DC}/2 + V_{OF}$, being V_{OF} the overshoot voltage [8] while the peak voltage on points B will be $2/3V_{DC}$. Hence, as long as $\frac{V_{DC}}{2} + V_{OF} \geq 2/3V_{DC}$, the phase to ground insulation will be stressed coherently with real operating scenarios, and the proposed method will hold. This scenario is verified when $V_{OF} \geq 1/6V_{DC}$, meaning an overshoot factor of at least 1.16, which is often found in common conditions.

Another important factor is that Joule and dielectric losses, despite being reduced, cannot be eliminated. Hence, the temperature set in the oven where tests are performed must be carefully chosen, so that the hotspot temperature inside the slot reaches the value selected for aging. Thermocouples in the machine slot or thermal imaging are thus necessary to control this process.

Finally, voltage reflections between the windings and the resistors may appear, influencing the transient voltage profile. The use of reflectometry analysis for matching the resistor impedance to the characteristic impedance of the windings will be explained in the next chapter.

IV. CASE STUDY

The first requirement of the modified setup is that the series resistors shall have negligible effects on the voltage waveforms across the first stator coils. Ideally, windings and resistors should share the same characteristic impedance to avoid reflections. Each phase winding of a rotating machine can be treated as a transmission line, characterized by its characteristic impedance. Indeed, the characteristic impedance of a rotating machine would change along the voltage wave path, meeting different stray parameters at various locations (e.g., straight part versus end-windings). As a first approximation, this aspect has been neglected. Since the theory to derive the characteristic impedance of the motor is based on a standard approach, the details are reported in Appendix.

A. CHARACTERISTIC IMPEDANCE ESTIMATION

The experiments were conducted on an 18-slot stator with concentrated windings, chosen for a proposed automotive electric drive application. Each phase consists of six coils connected in parallel. The stator has a diameter of 180 mm and a length of 300 mm. While the specific dimensions and winding configuration of the stator are unique to this study, the results are expected to be relevant to similar stator designs, such as a stator with a different number of slots, or distributed hairpin or double layer windings. The effect of coil geometry (number of turns, coil pitch) can significantly affect voltage distribution and transient response, as described in [22].

The converter used is a full-bridge 3-phase inverter based on SiC MOSFETS. It can generate voltage waveforms with an amplitude up to 1200 V, a rise time of 60 ns, and a switching frequency up to 22.5 kHz.

The S-parameter measurements necessary to derive the motor characteristic impedance were performed using an Agilent E5061B Vector Network Analyzer (VNA), for the frequency range between 50 Hz and 150 MHz. The instrument was calibrated, and the fixture used to connect the specimen to the instrument was properly compensated before each measurement.

Fig. 4 and Fig. 5 show the short circuit and open circuit impedance of the motor, which were used to derive the characteristic impedance Z_0 through (see Appendix):

$$Z_0 = \sqrt{Z_{SC} Z_{OC}} \tag{1}$$

The open circuit, short circuit, and characteristic impedance data, derived from S-parameter measurements, form the foundation for analyzing voltage transients and reflections. The characteristic impedance provides a baseline for matching impedance, reducing unwanted reflections.

The characteristic impedance derived from eqn. (1) is shown in Fig. 6. It is approximately 1 kΩ with a null phase in a broad range of frequencies, suggesting this as the more suitable value for the resistor to be inserted in series with each tooth coil. The rapid swings in Z_0 observed within the 100 kHz to 10 MHz range can be attributed to the interplay of inductances and capacitances in the end-winding and slot regions.

To provide insight into the individual coil's voltage profile, which is key to understanding the stress distribution during transients, Fig. 7 shows the voltages appearing across a tooth coil, its series resistor, and the series of the two elements. In this case, the resistor was the optimum one for a single coil,

that is, 1 $k\Omega$. Measurements were performed setting the DC bus voltage to 60V and using low-voltage, low-inductance resistors (these resistors could not be used in the final setup due to their low voltage specifications).

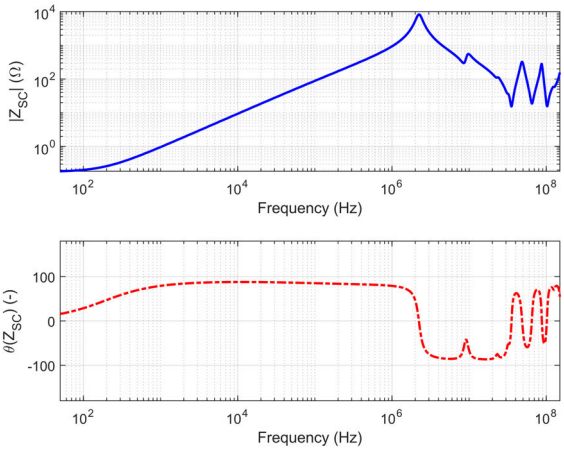

FIGURE 4. Short circuit impedance.

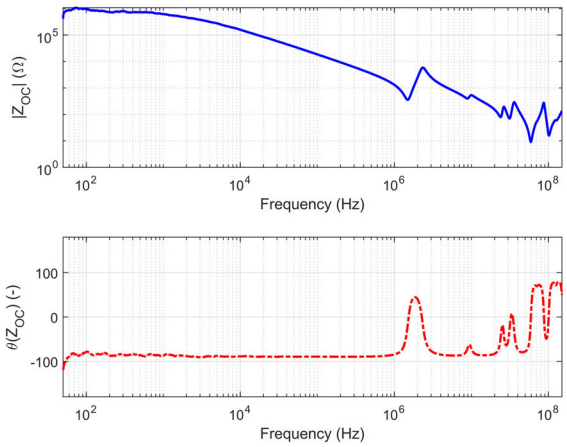

FIGURE 5. Open circuit impedance.

Fig. 7 shows that, as the voltage wave propagates through the coil, the high-frequency components of the voltage waveform are reduced [23]. Hence, for the sake of proper impedance matching, low-frequency components are more relevant than those at high frequencies.

While the machine impedance varies with frequency, this simplification reduces complexity. Its potential impact on stress distribution accuracy is mitigated by the attenuation of the high-frequency spectral components of the voltage due to machine losses. The overall effect of the resistor simplified choice is negligible, as proved by the limited reflections at the resistance terminals during testing.

B. BALANCING REFLECTIONS AND PRACTICAL LIMITATIONS

Testing on full stators can be done using various connection schemes. Two cases are shown in Fig. 8 for the winding

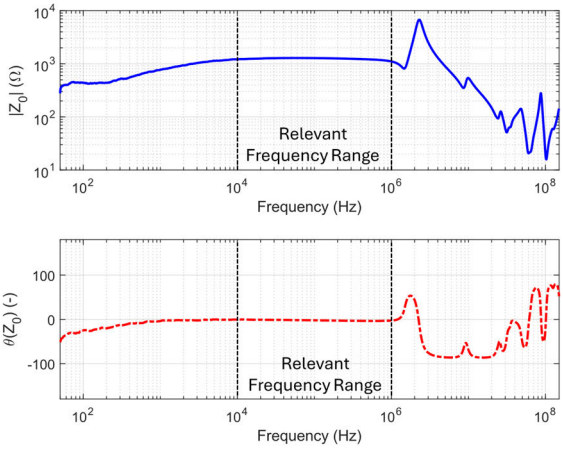

FIGURE 6. Characteristic impedance of approximately 1$k\Omega$ across the relevant frequency range.

discussed in this paper. In one case, each coil is connected in series with a resistor, as in Fig. 8(a). Alternatively, the six coils in one phase can be connected in parallel, and the parallel can be connected to a single resistor, as in Fig. 8(b). In the second case, the impedance to be used would be:

$$Z_0' = Z_0/n_p \tag{2}$$

where n_p is the number of windings connected in parallel (in this case, n_p= 6). However, this choice might lead to drawing excessive currents and overheating the system.

As a compromise, a series of measurements characterizing the voltage waveform distortion in the tooth coil using different values of series resistors was explored. This was done using low-voltage equipment. A pulsed waveform with a frequency spectrum like the one produced by the employed SiC converter was produced using a low-voltage signal generator.

Such a pulse was fed to the series composed of the tooth coil and a resistor. The voltage differential across the tooth was measured for different resistance values, and the results are shown in Fig. 9. For example, changing resistance from 1 $k\Omega$ to 1.25 $k\Omega$ still generates an acceptably low voltage ringing and, at the same time, reduces the current to acceptable values, if necessary.

In the case reported here, an 850 V DC bus with a current rating up to 0.8 A is used. This means that the minimum impedance of the overall system, composed of the whole stator windings and shunting resistors, should be 1062 Ω per phase. Consequently, the minimum resistance that could be used in each configuration would either be 3.2 kΩ (Fig. 8(a)), or 531 Ω (Fig. 8(b)).

On the other hand, the ideal resistor values that match the characteristic impedance and minimize waveform distortions are 1000 Ω and 166 Ω respectively. However, using these values would require a DC generator with larger ratings. As this solution could not be deployed shortly, the sensitivity of the coil voltages to the series resistance value was investigated, aiming at resistances larger than the optimum one.

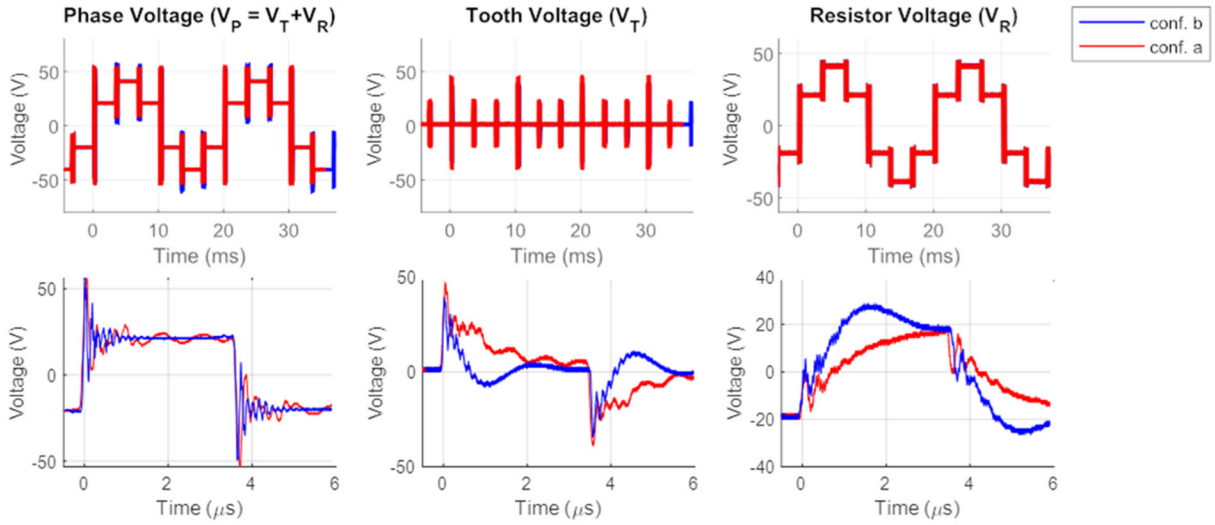

FIGURE 7. Comparison of the voltage appearing on the tooth coil and resistor, with a resistor in series having an optimal value according to reflectometry analysis and a sixth-fold value. V_P, V_T *and* V_R refer to the voltage drop across a single phase, one relative tooth coil, and resistor respectively.

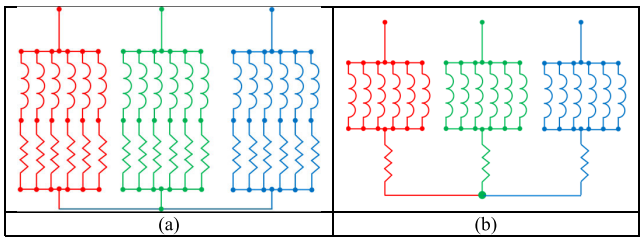

FIGURE 8. Possible resistor connection configuration.

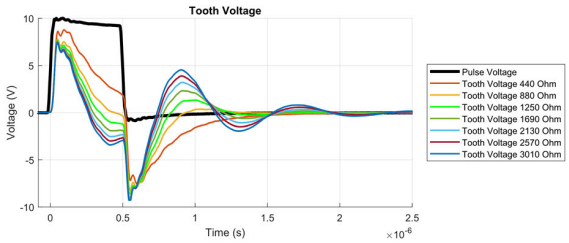

FIGURE 9. Voltage across a tooth coil, with various series resistances.

Experimental validation confirmed the theoretical characteristic impedance through observation of minimal reflected power during testing, indicating a close match between the test setup and the winding's inherent impedance. As shown in Fig.7, the peak voltage is reduced compared to that obtained under the optimal setup, reducing the turn-to-turn stress. However, such reduction is moderate (within 5%), and can be either considered acceptable, or compensated by mildly increasing the testing voltage. This mild reduction is associated with the fact that, while traveling in the coil, the voltage waveform rapidly loses its high-frequency content, as can be observed by inspecting the resistor voltages in Fig. 7. As a result, the sensitivity of the resistor value of the voltage applied to the insulation system is limited. While reflectometry provides a precise means of impedance matching, a trial-and-error approach can also be adopted for its accessibility and practicality, particularly for laboratories without access to specialized equipment.

A word of caution should be given about the resistor selection. Besides the resistance value, other resistor properties can be crucial: low parasitic parameters, sufficient maximum operating voltage and current, proper temperature range, and power dissipation. Indeed, all the active power will be dissipated mainly on resistors, which must be capable of withstanding both voltages, currents, and temperature. Installing the resistors on a suitable heatsink with a cooling system to limit the temperature is the best approach. Alternatively, direct installation of the resistors within the oven reduces the energy waste as the Joule losses will be used to heat the oven. However, this solution requires resistors with extremely high operating temperatures.

In conclusion, the best resistance value obtained according to the reflectometry analysis might feature a set of characteristics difficult to find on the market. However, the experimental evidence suggests that even a significant difference between theoretical and practical resistor values only modestly affects the voltages, giving a good margin for its selection, allowing for proper testing under the given practical limitations.

While fundamentally scalable, adapting and validating this approach for more complex systems would require significant modifications. Hairpin designs, for example, with their reduced inductance and overall characteristic impedance, pose a particular challenge, necessitating adjustments to resistor values and potentially incorporating distributed impedance matching techniques.

V. PRELIMINARY QUALIFICATION RESULTS

The waveshapes shown in Fig. 3 were obtained using a DC bus voltage of 850 V and a 500 Ω resistor per phase (see Fig. 8(b)), which is approximately three times higher than the optimal value determined by reflectometry. Initially, the oven temperature was set to 120°C to perform a preliminary assessment of the difference between thermal and electro-thermal aging.

After 300 hours of aging, the test was interrupted, and PDIV measurements were carried out periodically through momentary interruptions of the aging test, utilizing a dedicated partial discharge measurement system. The PDIV had reduced by about 10%, from a range of 3.44 − 3.39 kVpk to 3.09 − 3.0 kVpk. Interestingly, tests performed on a statorette subjected only to thermal aging did not show a PDIV reduction in the same period. It is speculated that, under combined electrothermal stress, PD activity occurred in the system, leading to a degradation of the insulation, with the reduction of the PDIV. On the contrary, thermal aging under the same temperature did not cause any issue to the insulation. Those results highlight the necessity for testing under multi-factor aging conditions.

After this preliminary test, the oven temperature increased to 150°C. After 1 hour from the start of the tests, it was observed that the DC voltage had decreased and the current had reached the maximum of the supply system, i.e., 1 A. This could be explained assuming that the DC supply had limited the voltage to control the current to its maximum value, indicating a reduction of the load impedance. Thermal imaging revealed that the temperature of the stator mockup reached about 200°C, and part of the insulation had melted. Since the current-limiting resistors were held outside the oven, the only possible explanation for this phenomenon was an increase of the dielectric losses associated with a too-high temperature of the oven, which had caused part of the insulation to exceed the glass transition temperature, reaching large values of the dissipation factor.

After failure, dielectric properties, including tan(δ), were measured across a range of frequencies on a pristine twin stator, revealing elevated loss levels around 10 kHz. These features helped explain the observed insulation melting at 150°C and established a baseline understanding of the material's limitations. These detailed results are not extensively documented in this paper to maintain focus on the methodology.

VI. CONCLUSION

An approach to apply temperature and voltage to inverter-fed electric motor insulation models is proposed in this paper. This approach resorts to the use of the inverter drive and current-limiting resistors. A proper design of these resistors allows for limiting the supply current despite the lack of the back electromotive force due to the rotor while applying voltages resembling those experienced in operation.

Electro-thermal aging during qualification of inverter-fed electrical machines enables the synergies between electrical and thermal stress to be activated, something which are not accounted for by sequential testing. Under modern wide bandgap inverters, electro-thermal testing can bring the insulation to failure in relatively short times when the applied voltage exceeds the PDIV. Thus, this approach can make superfluous the diagnostic cycle for Type I (organic) machines. Besides, failure by thermal runaway can also be observed, leading to a better understanding of the temperature limits of the machine under overload.

The proposed approach might be somewhat intimidating as it seems to need a VNA to find the optimal resistor value. Indeed, results have shown that the voltage applied to the insulation is relatively insensitive to the value of the resistor. This might suggest that a simple trial-and-error approach can suffice to design the test setup.

While the presented method primarily focuses on simulating rotor-less operation within a limited test setup, the insights gained about voltage distribution and the impact of series resistance offer a foundational understanding applicable to broader stator testing scenarios and contribute to a more complete characterization of insulation behavior under controlled conditions. The fundamental principles can also inform the design of more sophisticated testing equipment.

To further confirm the procedure and compare results to IEC 60034-18-21, more testing on various stator designs is planned, alongside detailed comparisons with simulations and theoretical models.

APPENDIX
DERIVATION OF MOTOR CHARACTERISTIC IMPEDANCE

The solution of the Telegrapher's equations:

$$V(x) = V^{+}e^{-\gamma x} + V^{-}e^{\gamma x} \tag{A.1}$$

$$I(x) = I^{+}e^{-\gamma x} + I^{-}e^{\gamma x} \tag{A.2}$$

provide the input impedance Z_{IN} of a transmission line with constant characteristic impedance and length d:

$$Z_{IN} = \frac{V(0)}{I(0)} = Z_0 \frac{Z_L + Z_0 \tanh(\gamma d)}{Z_0 + Z_L \tanh(\gamma d)} \tag{A.3}$$

where γ is the propagation constant of the line, Z_0 and Z_L are the characteristic impedance of the line and the load at the end of it, respectively. As a first approximation, this approach can be used to derive the characteristic impedance of the motor.

The length d, under the mentioned approximation is the length of the voltage wave path in the conductors.

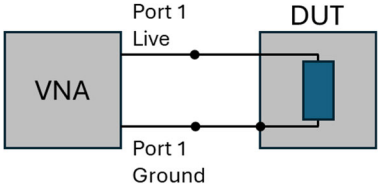

FIGURE 10. Scheme for reflectometry measurements.

Considering equation Eq. (A.3) for short circuit and open circuit loads, the following equations are obtained:

$$Z_L = 0 \rightarrow Z_{IN} = \frac{Z_0}{\tanh(\gamma d)} = Z_{SC} \tag{A.4}$$

$$Z_L = \infty \rightarrow Z_{IN} = Z_0 \tanh(\gamma d) = Z_{OC} \tag{A.5}$$

The value of the characteristic impedance Z_0 is obtained from Eq. (A.4) re-substituted into Eq. (A.5), also obtaining the propagation constant value:

$$Z_0 = \sqrt{Z_{SC} Z_{OC}} \tag{A.6}$$

$$\gamma = \frac{1}{d} \tanh^{-1}\left(\sqrt{\frac{Z_{SC}}{Z_{OC}}}\right) \tag{A.7}$$

The short-circuit and open-circuit impedance needed for the calculation can be determined from measurements of the S-parameters and from the reflection coefficient, which can be measured by reflectometry. Since the parameter S_{11} is equal to the reflection coefficient Γ_{IN}:

$$S_{11} = \Gamma_{IN} = \Gamma_L e^{-2\gamma d} \tag{A.8}$$

and knowing the characteristic impedance of the measurement equipment (Z_L, usually 50Ω):

$$Z_{OC} = 50 \times \frac{1 + S_{11,OC}}{1 - S_{11,OC}} \tag{A.9}$$

$$Z_{SC} = 50 \times \frac{1 + S_{11,SC}}{1 - S_{11,SC}} \tag{A.10}$$

REFERENCES

[1] D. Aliprantis and S. Pekarek, "The unsung hero of the electric vehicle revolution: The role of computational electromagnetics in electric machine design and analysis," *IEEE Electrific. Mag.*, vol. 11, no. 4, pp. 64–68, Dec. 2023, doi: 10.1109/MELE.2023.3320510.

[2] I. Husain, B. Ozpineci, M. S. Islam, E. Gurpinar, G.-J. Su, W. Yu, S. Chowdhury, L. Xue, D. Rahman, and R. Sahu, "Electric drive technology trends, challenges, and opportunities for future electric vehicles," *Proc. IEEE*, vol. 109, no. 6, pp. 1039–1059, Jun. 2021, doi: 10.1109/JPROC.2020.3046112.

[3] C. H. T. Lee, W. Hua, T. Long, C. Jiang, and L. V. Iyer, "A critical review of emerging technologies for electric and hybrid vehicles," *IEEE Open J. Veh. Technol.*, vol. 2, pp. 471–485, 2021, doi: 10.1109/OJVT.2021.3138894.

[4] V. Madonna, P. Giangrande, and M. Galea, "Electrical power generation in aircraft: Review, challenges, and opportunities," *IEEE Trans. Transport. Electrific.*, vol. 4, no. 3, pp. 646–659, Sep. 2018, doi: 10.1109/TTE.2018.2834142.

[5] M. Lukic, P. Giangrande, A. Hebala, S. Nuzzo, and M. Galea, "Review, challenges, and future developments of electric taxiing systems," *IEEE Trans. Transport. Electrific.*, vol. 5, no. 4, pp. 1441–1457, Dec. 2019, doi: 10.1109/TTE.2019.2956862.

[6] M. Doppelbauer and P. Winzer, "A lighter motor for tomorrow's electric car," *IEEE Spectr.*, vol. 54, no. 7, pp. 26–31, Jul. 2017, doi: 10.1109/MSPEC.2017.7951719.

[7] S. Nuzzo, D. Barater, C. Gerada, and P. Vai, "Hairpin windings: An opportunity for next-generation E-motors in transportation," *IEEE Ind. Electron. Mag.*, vol. 16, no. 4, pp. 52–59, Dec. 2022, doi: 10.1109/MIE.2021.3106571.

[8] *Rotating Electrical Machines—Part 18-41: Partial Discharge Free Electrical Insulation Systems (Type I) Used in Rotating Electrical Machines Fed From Voltage Converters-Qualification and Quality Control Tests*, Standard IEC 60034-18-41, International Electrotechnical Commission, Geneva, Switzerland, 2019.

[9] *Turn-to-Turn Converter Stress Impact on the Lifetime of Rotating Machines | IEEE Conference Publication | IEEE Xplore*. Accessed: Mar. 26, 2024. [Online]. Available: https://ieeexplore.ieee.org/document/10410546

[10] A. Cavallini, G. C. Montanari, and L. E. Mariut, "The influence of test voltage waveforms on partial discharge activity in XLPE," in *Proc. IEEE Int. Symp. Electr. Insul.*, Jun. 2012, pp. 554–557, doi: 10.1109/ELINSL.2012.6251531.

[11] P. Seri, G. C. Montanari, and R. Hebner, "Partial discharge phase and amplitude distribution and life of insulation systems fed with multilevel inverters," in *Proc. IEEE Transp. Electrific. Conf. Expo. (ITEC)*, Jun. 2019, pp. 1–6, doi: 10.1109/ITEC.2019.8790563.

[12] T. J. Å. Hammarström, "Partial discharge characteristics at ultra-short voltage risetimes," *IEEE Trans. Dielectr. Electr. Insul.*, vol. 25, no. 6, pp. 2241–2249, Dec. 2018, doi: 10.1109/TDEI.2018.007445.

[13] M. Pastura, S. Nuzzo, F. Immovilli, A. Toscani, A. Rumi, A. Cavallini, G. Franceschini, and D. Barater, "Partial discharges in electrical machines for the more electric aircraft—Part I: A comprehensive modeling tool for the characterization of electric drives based on fast switching semiconductors," *IEEE Access*, vol. 9, pp. 27109–27121, 2021, doi: 10.1109/ACCESS.2021.3058083.

[14] *Rotating Electrical Machines—Part 18-21: Functional Evaluation of Insulation Systems–Test Procedures for Wire-Wound Windings-Thermal Evaluation and Classification*, Standard IEC 60034-18-21, International Electrotechnical Commission, Geneva, Switzerland, 2012.

[15] *Evaluation and Qualification of Electrical Insulation Systems*, Standard IEC 60505, International Electrotechnical Commission, Geneva, Switzerland, 2011.

[16] T. Hammarstrom, "Influence of PD characteristics within motor windings exposed to elevated temperatures," in *Proc. Int. Symp. Electr. Insulating Mater. (ISEIM)*, Sep. 2023, pp. 324–327, doi: 10.23919/iseim60444.2023.10329024.

[17] A. Rumi, P. Seri, and A. Cavallini, "Electric field distribution at high temperatures in impregnated enameled conductors used in electrical machines," in *Proc. Int. Symp. Electr. Insulating Mater. (ISEIM)*, Sep. 2023, pp. 1–4, doi: 10.23919/iseim60444.2023.10329189.

[18] V. Madonna, P. Giangrande, L. Lusuardi, A. Cavallini, C. Gerada, and M. Galea, "Thermal overload and insulation aging of short duty cycle, aerospace motors," *IEEE Trans. Ind. Electron.*, vol. 67, no. 4, pp. 2618–2629, Apr. 2020, doi: 10.1109/TIE.2019.2914630.

[19] V. Madonna, P. Giangrande, and M. Galea, "Phase to ground insulation in low voltage machines: Lifetime evaluation under enhanced thermal stress," in *Proc. 10th Int. Conf. Power Electron., Mach. Drives (PEMD)*, vol. 2020, Dec. 2020, pp. 361–366, doi: 10.1049/ICP.2021.1128.

[20] M. Kaufhold, H. Aninger, M. Berth, J. Speck, and M. Eberhardt, "Electrical stress and failure mechanism of the winding insulation in PWM-inverter-fed low-voltage induction motors," *IEEE Trans. Ind. Electron.*, vol. 47, no. 2, pp. 396–402, Apr. 2000, doi: 10.1109/41.836355.

[21] W. Yin, "Failure mechanism of winding insulations in inverter-fed motors," *IEEE Elect. Insul. Mag.*, vol. 13, no. 6, pp. 18–23, Nov. 1997, doi: 10.1109/57.637150.

[22] R. S. Ferreira and A. C. Ferreira, "Analysis of end-windings influence on the transient voltage distribution in machine stator windings by a three phase model," *IEEE Trans. Energy Convers.*, vol. 36, no. 3, pp. 2110–2119, Sep. 2021, doi: 10.1109/TEC.2020.3037453.

[23] A. Cavallini, E. Lindell, G. C. Montanari, and M. Tozzi, "Off-line PD testing of converter-fed wire-wound motors: When IEC TS 60034-18-41 may fail?" *IEEE Trans. Dielectr. Electr. Insul.*, vol. 17, no. 5, pp. 1385–1395, Oct. 2010, doi: 10.1109/TDEI.2010.5595540.

A. RUMI received the B.Sc., M.Sc., and Ph.D. degrees (Hons.) in electrical engineering from the University of Bologna, in 2016, 2019, and 2023, respectively. He is currently a Product Manager with the Flexible Insulation Division, Coveme S.p.A. His research activities focus on the characterization of advanced insulation systems, with emphasis on partial discharge analysis and lifetime assessment. His work also includes discharge modeling, dielectric material diagnostics and analysis, aging mechanisms investigation, and reliability evaluation. His broader interests include HVdc cable insulation, piezoelectric materials for sensing and energy harvesting, and packaging solutions for power electronics.

L. ZANOTTI received the B.Sc. and M.Sc. degrees (Hons.) in electrical engineering from the University of Bologna, in 2019 and 2022, respectively. He is currently an Electrical Design and Testing Engineer in electrical systems and automated machinery. His experimental activity focused on the characterization of insulation systems for low-voltage rotating machines fed by converters based on wide-bandgap devices. His research interests include the diagnosis of insulation systems through partial discharge analysis, and the development of a test bench for vehicle powertrains to analyze ageing behaviors of its insulation systems under combined thermal, electrical, and mechanical stress.

A. CAVALLINI (Fellow, IEEE) is currently a Full Professor with the University of Bologna. His main research interests are focused on partial discharge phenomena in power system equipment and in electrical drives used for transport electrification. He is the co-author of about 280 scientific articles and 15 international patents and the co-founder of University spin-off Techimp. He is an active in the IEEE DEIS (an Adcom Member, the Transport Electrification Technical Committee Chair, the Education Committee Chair, and the DEIS Italy Chapter Chair), CIGRE (convener of D1.43 and D1.74, formerly Italian representative in SC D1), IEC TC 2 MT 10 (Italian representative), and SAE.

P. SERI (Member, IEEE) received the Ph.D. degree in electrical engineering from the University of Bologna, in 2016. In 2017, he was with the Laboratory of Innovative Materials for Electrical Systems (LIMES), University of Bologna, as a Research Fellow. He is also a Researcher with the Department of Electrical, Electronic, and Information Engineering, DEI, University of Bologna. He is working on the topics of HVdc cables design, partial discharge detection and modeling, and characterization of dielectric materials.